Charge Regulated Diffusion of Silica Nanoparticles into Wood for Flame Retardant Transparent Wood

ADVANCED SUSTAINABLE SYSTEMS
www.advsustainsys.com

Charge Regulated Diffusion of Silica Nanoparticles into Wood for Flame Retardant Transparent Wood

Archana Samanta, Martin Höglund, Pratick Samanta, Sergei Popov, Ilya Sychugov, Lorenza Maddalena, Federico Carosio, and Lars A. Berglund*

The preparation of wood substrates modified by charged inorganic nanoparticles (NPs) diffusing into the internal cell wall structure is investigated for generating functional properties. The flammability problem of wood biocomposites is addressed. NPs applied from colloidal sols carry charge to stabilize them against aggregation. The influence of charge on particle diffusion and adsorption should play a role for their spatial distribution and localization in the wood substrate biocomposite. It is hypothesized that improved dispersion, infiltration, and stability of NPs into the wood structure can be achieved by charge control diffusion, also restricting NP agglomeration and limiting distribution to the wood cell wall. Cationic and anionic silica NPs of ≈30 nm are therefore allowed to diffuse into bleached wood. The influence of charge on distribution in wood is investigated as a function of initial sol concentration. Transparent wood is fabricated by in situ polymerization of a thiol-ene in the wood pore space. These biocomposites demonstrate excellent flame retardancy with self-extinguishing characteristics. The approach has potential for commercial fabrication of flame retardant transparent composites for glazing and other building applications.

1. Introduction

Cellulosic materials are of paramount interest for advancing sustainable technologies.[1,2] Wood is of particular interest as a widely available renewable resource with high ratio of mechanical properties to density, suitable for large, eco-friendly load-bearing structures.[3–5] The wood structure can be viewed as a reinforcement framework combining micro- and mesoscale porosity, along with anisotropic hierarchical structure dominated by oriented cellulose nanofibers; which provides many opportunities for functionalization of the nanoporous wood cell wall.[6–9] Wood substrates can be filled by polymer to fabricate transparent wood (TW) composites of high transparency, tunable optical properties, and strongly enhanced mechanical properties compared to neat polymers.[10–13] Nanoparticle (NP) functionalization of wood has gathered significant attention, in particular for advanced applications.[14,15] Examples of TW functionalization include optical responsiveness, energy conservation, and luminescent properties.[16]

Fabrication of TW requires removal of coloring substance from the wood scaffold. The brownish color of wood is primarily attributed to presence of lignin chromophores.[17] The current approach for fabricating transparent wood is based on chlorine-free hydrogen peroxide bleaching instead of the conventional delignification technique. Delignification processes may generate odorous components, such as methyl mercaptan, dimethyl sulfide, and hydrogen sulfide for example, but may also produce toxic effluents such as chlorinated dioxins.[18] The process is time-consuming and not necessarily environmentally friendly. In contrast, hydrogen peroxide bleaching is totally chlorine-free with shorter processing times compared to delignification. Delignification often results in 90% loss of lignin which reduces mechanical properties of the wood scaffold, affecting the handing and fabrication of large substrates.[19] Bleaching, on the other hand, removes chromophoric structures with 80% retainment of lignin, thereby produces wood substrates with better structural integrity and improved mechanical properties compared to delignified wood substrates.

Here, we investigate the possibility to bring electropositive silica NPs into the nanostructured wood cell wall of the bleached wood by electrostatic interaction, as a preparation strategy for wood nanotechnologies. The feasibility as well as the benefits of controlled nanostructure and NP distribution is demonstrated by strongly reduced flammability of TW.

Functional particles for TW modification are commonly added to a liquid monomer mixture and impregnated into the wood structure followed by polymerization.[20] Problems may include inhomogeneous particle distribution, passivation from monomer chemistry and agglomeration. One alternative is NP

A. Samanta, S. Popov, I. Sychugov
Department of Applied Physics
KTH Royal Institute of Technology
Stockholm 11419, Sweden
E-mail: archanas@kth.se
M. Höglund, P. Samanta, L. A. Berglund
Department of Fiber and Polymer Technology
Wallenberg Wood Science Center
KTH Royal Institute of Technology
Stockholm 10044, Sweden
L. Maddalena, F. Carosio
Politecnico di Torino
Alessandria Site, Viale Teresa Michel 5, Alessandria 15121, Italy
The ORCID identification number(s) for the author(s) of this article can be found under https://doi.org/10.1002/adsu.202100354.

DOI: 10.1002/adsu.202100354

precipitation from solution, although this provides less control of NP shape and function.[21,22] There may also be leaching problems.[23] For successful modification inside the wood cell wall, it is essential to swell the cell wall so that it becomes accessible.[24] To facilitate NP infiltration into the wood substrate and inside the cell wall, we use a fully aqueous system under basic conditions. This approach should be scalable, show increased NP diffusion rates and allow high NP content.

Many commercially available NP dispersions are surface stabilized by repulsive charges.[25–27] Very few studies have investigated the diffusion of NPs in wood related to their surface chemistry. Segmehl et al. studied the diffusion pattern of water in the cell wall based on the migration behavior of ultrasmall europium-doped hafnium dioxide particles traced by Raman microscopy.[28] The diffusion of NPs, however, also depends on size, aggregation tendency, and charge density, which is yet to be explored. Jun et al. studied the influence of pH on aggregation tendencies of anionic silica NPs and their migration into wood structures. It was observed that higher pH resulted in particle aggregation from ≈25 to 300 nm, which influenced the NP weight fraction in the wood structure.[29] Here we select designed cationic silica NPs, which may show favorable diffusion behavior into anionic wood cell walls. The influence of charge and charge density is explored especially in high NP concentration regions where NP aggregation is a well-known problem which limits the extent of wood functionalization.

Cationic silica (SiO_2) sol containing ≈30 nm particles dispersed in water are allowed to diffuse inside bleached wood. The combination of silica particles and regenerated cellulose resulted in interesting properties where the chemical similarity in terms of hydroxylated surfaces was deemed favorable.[30] Silica is ecofriendly in the sense of its abundance, and cellulose-silica composites have been studied for protection against fungal decomposition, gas separation, etc.[31–36] Cellulose and its derivatives have also been used in combination with silica particles for aerogels, desalination membranes, membranes for oil water separation, films for passive radiative cooling, filters for cigarette smoke, thermal insulation etc.[37–43] A straightforward process to facilitate infiltration and achieve homogenous distribution of silica into cellulose can enhance the processibility and scalability for fabrication of these functional materials.

Here, bleached birch wood veneer was used as the cellulosic wood substrates and modified by silica NPs to fabricate TW composites. Silica sols containing the dispersed cationic or anionic NPs were used. The pH of the colloidal sol was kept at 8.5 to preserve the silica NPs, since cold alkali could dissolve amorphous silica above pH 10.3.[44] This also induces wood cell wall swelling.

The functionality of silica NPs in the wood substrate was tested by fabrication of TW examined for flame retardancy. Flame retardant properties of wood is an important problem where toxic additives dominate current technologies. Coating of wood by flame retardants is most commonly used technique.[45–49] Zinc, phosphorous or metallic salts or chlorinated or brominated biphenyls and ethers diphenyl have been used.[50–53] The risk for leaching and toxic environmental effects is a significant limitation.[54,55] Here we show that eco-friendly silica sols impregnated inside the composite unlike surface coating can render transparent wood or other biocomposites to become self-extinguishing and flame retardant.

2. Results and Discussion

2.1. Wood-Silica NP Interactions

First, the effect of silica NP charge on impregnation into porous wood substrates is investigated. The colloidal stability of silica sols was investigated by comparing particle size and zeta potentials of the formulations. Cationic and anionic silica sols with size of 30 ± 5 nm, showed zeta potential values of 50.1 ± 0.2 and −47.9 ± 0.4 mV, respectively. The values remained unchanged (<1%) when NP size and zeta potential were again assessed after 48 h. For the NP impregnation experiments, particle agglomeration is therefore not a concern.

The wood tissue in the substrates is electronegative. Carboxylic acids in the wood cell wall are deprotonated during infiltration at pH 8.5.[56,57] Deprotonation swells the wood cell wall, where the cellulose nanofibers are preserved in a swollen aqueous gel of hemicellulose and lignin. Wood cell wall accessibility is therefore increased, while the hierarchical nature of the wood structure and microscale porosity at the center of wood fiber cells ("lumen") are preserved, see **Scheme 1**a. Ionic interactions are foreseen between the cationic silica and anionic cell wall sites and should provide more homogenous silica distribution inside the wood substrate. Negatively charged carboxyl groups are derived from native hemicelluloses as well as created during the bleaching step.[58] The oppositely charged silica particles are expected to form ionic bonds with the anionic sites in wood, which could promote silica infiltration and neutralize the charge of bleached wood, see Scheme 1b. Note that after silica NP impregnation, the functionalized wood substrate will be fully impregnated by a polymer precursor liquid, and polymerized in-situ to form a TW biocomposite.

The correlation between NP charge, diffusion and impregnation of the wood substrate was investigated by equilibrium impregnation at different NP colloidal sol concentrations. The higher the gradient in sol charge density (regulated by silica concentration), the shorter the neutralization time for wood samples when immersed in cationic silica sol. A maximum concentration of 2 M silica sol was used before the NPs started to aggregate. **Figure 1**a,b represents the change in charge density of the silica sols with time, before and after impregnation, while maintaining a wood to silica sol weight ratio of 1:5. Note that the bleached birch substrates have a charge of −165 ± 10 μeq. g^{-1} at pH 8.5.

The charge density in the cationic sols dropped with impregnation time for all concentrations, whereas charge density of anionic sols remained unaltered even at different concentrations of the sol, shown in Figure 1a,b. Note that a drop of 165 ± 10 μeq. g^{-1} is observed in all cationic sol treated wood samples irrespective of initial sol concentration. Apparently, this drop is related to the charge of bleached birch wood. The equilibrium charge neutralization period is achieved in 6, 12, and 24 h in cationic sols with 2, 1, and 0.17 M concentrations, respectively. This result is in agreement with previous studies, indicating that the diffusion flux of diffusing species (here silica NPs) is

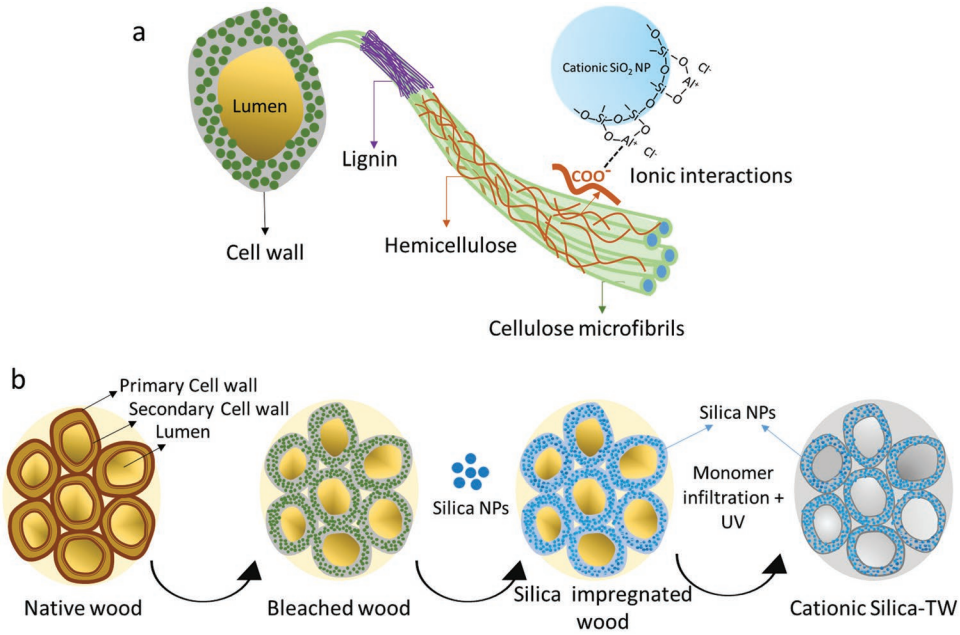

Scheme 1. Illustration of a) ionic interactions between oppositely charged wood sites and silica NPs and b) mechanism of silica infiltration and formation of TW biocomposites. "Lumen" is the central space in wood fiber cells. The "Cell wall" is the solid wall of the tubular wood fiber cell. The green dots in the cell wall are symbolizing cellulose microfibrils (or "cellulose nanofibers"). In "Bleached Wood" the chromophores in lignin have been removed chemically.

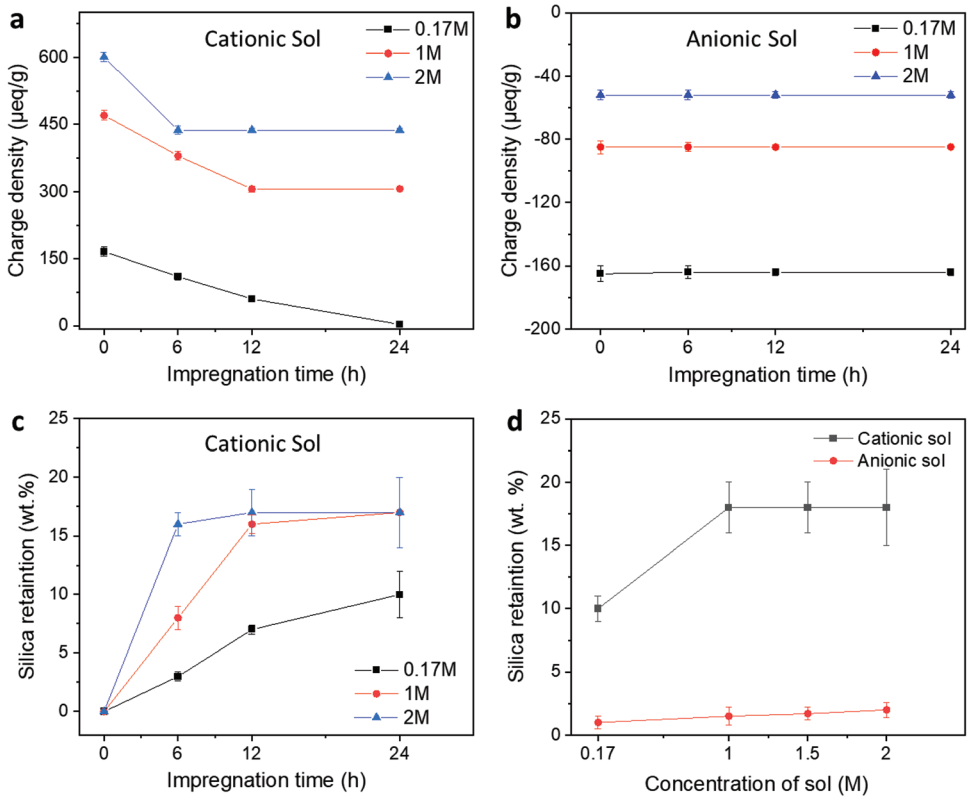

Figure 1. Influence of silica NP charge density on silica retention after uptake in anionic birch substrates and washing. Charge density changes of a) cationic and b) anionic silica sol impregnated into bleached birch, c) dry content of silica retained in the template as a function of impregnation time in bleached wood impregnated with cationic sol, and d) dry content of silica retained in the bleached wood template as a function of silica sol concentration with impregnation time of 24 h.

proportional to the concentration gradient of charged silica in this system (wood and the sol).[59] With the possibility to use higher concentration, we can speed up processing.

To verify the influence of charge density on NP diffusion, the weight of silica remaining inside the wood substrate was assessed after multiple washing steps, see Figure 1c,d. The uptake of cationic silica (Figure 1c) follows a similar trend as that of charge neutralization, and electrostatic interactions are controlling silica uptake. At saturation, 18 ± 5 wt% is retained at 1 M concentration of cationic silica sol, see Figure 1d, and increased silica concentration (2 M) does not enhance the uptake further. Anionic silica sols showed negligible silica uptake due to repulsion effects with the wood substrate. A silica uptake of < 2 wt% was observed, possibly from entrapment of silica within the intricate structures of wood.

The distribution of infiltrated silica NPs across the freeze fractured cross-section of the wood cell wall was analyzed. **Figure 2**a shows homogenously distributed silica NPs inside the birch cell walls for the cationic case. This is a very important result, which confirms diffusion of silica NPs inside the nano- and mesoporous space of the wood cell wall during sol impregnation. In contrast, the anionic sols did not show any NPs retention inside the wood cell wall (Figure S1, Supporting Information).

There were also concentration effects. The samples impregnated by 1 and 2 M cationic sol appeared to be "saturated" with silica NPs, whereas regions with no silica NPs were observed for 0.17 M cationic silica samples. The charge density of cationic 0.17 M sol was similar to the charge neutralization value for the anionic birch (−165 ± 10 μeq. g^{-1}), which may not be sufficient for effective diffusion into the wood substrate. This is supported by low silica content (≈10 wt%) for the cationic 0.17 M sol compared to the saturation gain of ≈18 wt% in samples impregnated by 1 and 2 M cationic sols (Figure 1c).

For more detailed information on spatial distribution of silica NPs, energy dispersive spectroscopy (EDS) mapping and point analysis were carried out, see Figure 2b. A uniform distribution of silica is observed inside the freeze-fractured cross-section of the cell wall for wood treated by cationic sol (1 and 2 M). EDS point analysis (Figure S2, Supporting Information) demonstrated homogeneous silicon content and distribution in the wood tissue, with no evident difference between the middle lamella and the secondary cell wall. The anionic NP wood samples showed sparse regions of silicon and oxygen peaks inside cell wall pores remaining after washing. Elemental silicon content, however, was very low (< 2 wt%) in line with results in Figure 1d.

As an additional confirmation of silica presence in the wood cell wall, FTIR-data are shown in Figure S3(a) (Supporting Information). The presence of the characteristic Si—O stretching peak at 1109 cm^{-1} in the bleached birch treated with 2M of cationic silica are in support of silica in the wood cell walls.[29] The normalized intensity of carboxyl stretch peak at 1728 cm^{-1} (C=O stretching of the carboxyl group) (Figure S3(b) (Supporting Information)) was reduced in cationic silica treated samples compared to bleached birch or birch anionic silica samples, as expected from charge neutralization of bleached birch by oppositely charged cationic silica NPs.[60–62]

The procedure for homogeneous impregnation of wood substrates with silica NPs is thus established. The next step is to introduce a polymer matrix phase and fabricate a flame-retardant transparent biocomposite, in the form of TW, see (Scheme 1b). Sample codes of are provided in **Table 1**. Silica NPs are only distributed in the wood substrate cell walls and not in lumen space at the center of wood cells, see TW – Cat 2M sample, Figure 2b.

2.2. Silica Effects on Polymerization of TW Composites

The in situ polymerization was not affected by the presence of NPs in the template. This is based on Raman peak analysis of the degree of cure of thiols and allyl monomers (-enes), see the Experimental Section and spectra in **Figure 3**a.[63] The results show similar degree of cure in the TW composites as compared with the polymerized neat thiol-ene TW, **Table 2**.

2.3. Optical Properties of Silica – TW Composites

The basic optical properties for TW composites are transmittance and haze. The influence of silica NPs on these properties was evaluated, see Figure 3b,c. Transparency and haze at 550 nm of control TW samples were observed to be 86 ± 2 and 50 ± 0.5%, respectively. The drop in transmission values for TW – Cat 2M was only 5% at 550 nm with silica addition as compared to the control TW. The drop is obviously lower for anionic NPs, since the silica content is much lower. Similarly, the haze of TW – Cat 2M is also increased slightly (9.7 ± 0.2% at 550 nm) compared with the control TW composites. Silica NPs are scattering light, despite their small size, since their refractive index (1.45) is different from the RI of thiol-ene (1.56) and the wood substrate (1.54). The transmittance and haze of TW composites containing cationic NPs have sufficiently good values to allow additional functionalization for photonics applications.[64]

2.4. Mechanical Properties of Silica – TW Composites

The mechanical properties of the TW composites were evaluated to assess the influence of silica on the properties of the control TW. **Figure 4**; and Table S1 (Supporting Information) show that the silica NPs enhanced the mechanical properties by a moderate extent. Neat thiol-ene film showed a tensile strength and modulus of 46.5 ± 2 MPa and 2.0 ± 0.2 GPa, respectively. Control birch thiol-ene TW composite with 28 ± 2 wt% wood reinforcement showed substantially enhanced tensile strength and modulus of 179 ± 5 MPa and 12.3 ± 0.4 GPa, respectively. Inclusion of silica NPs in the wood substrate resulted in enhancement of tensile strength and modulus to 189 ± 4 MPa and 13.7 ± 0.3 GPa, respectively (TW – Cat 2M). No observable effects were observed in the TW – An 2M samples because of the low silica NP content (Table 1).

To support this observation, additional composites from balsa wood were impregnated with 2 M cationic or anionic silica sols and TW were fabricated in the same process as explained in the Experimental Section. Control balsa – TW (with 12 ± 2 wt% wood and 88 ± 2 wt% thiol-ene content) showed a tensile strength and modulus of 60.7 ± 2 MPa and 3.6 ± 0.4 GPa,

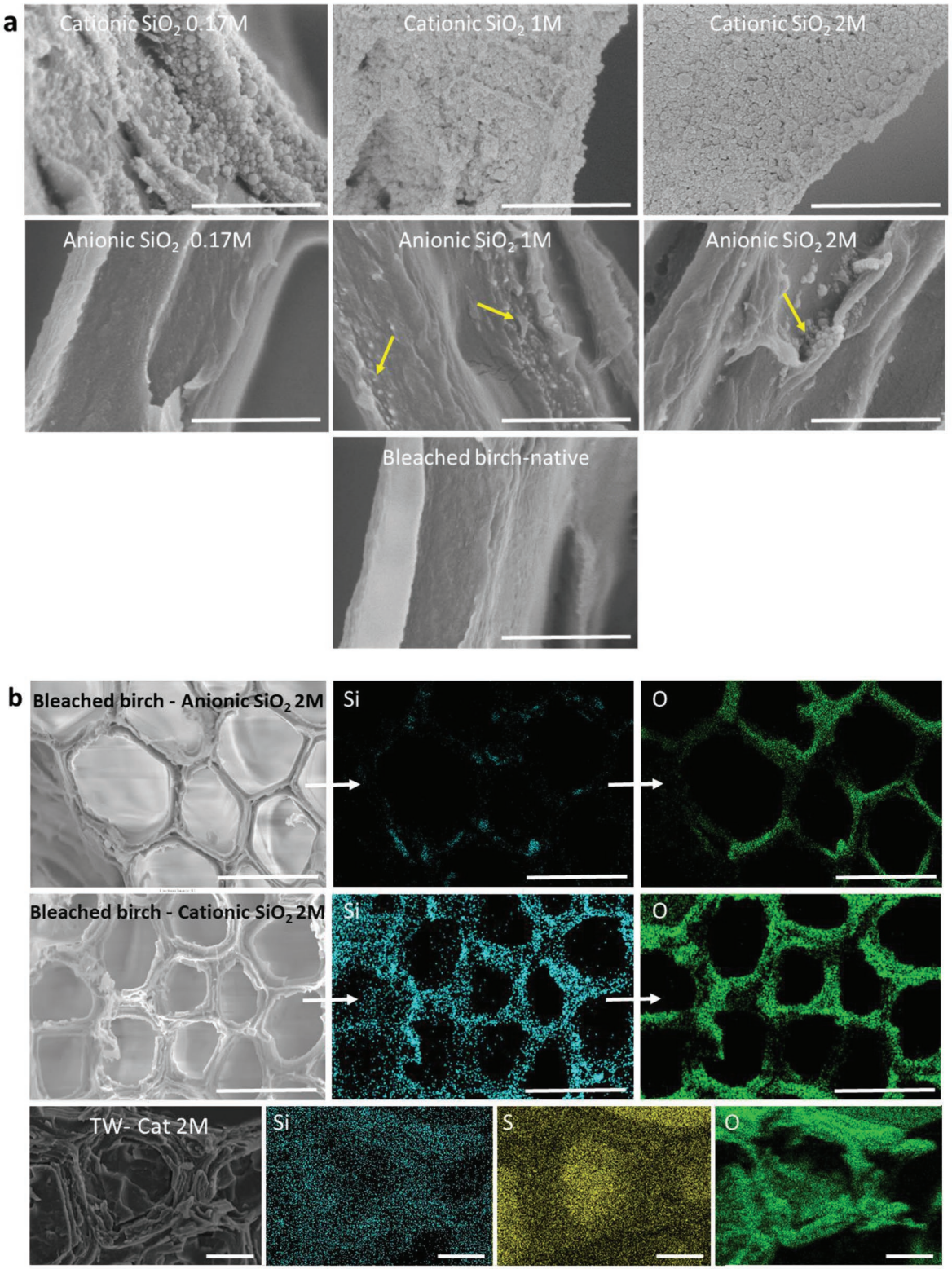

Figure 2. Surface characteristics of bleached birch samples impregnated with silica sols. a) SEM and b) EDS mapping. The white bars in a) and b) indicate a scale of 1 and 20 μm, respectively. SEM micrographs and EDS maps show almost complete silica coverage of the cell wall surface for cationic 1 and 2 M sols. Anionic sols only achieved localized adsorption of silica NPs. EDS mapping of TW composites made from cationic 2 M wood templates show retention of silica NPs in the cell wall. The sulfur signal tracks the thiol-ene distribution, which primarily fills the lumen of the wood templates, and can be used as a negative image of the cell wall.

Table 1. Sample designations for silica TW composites. The polymer phase is Thiol-ene.

Sample code	Silica treatment	Wood [wt%]	Silica [wt%]	Thiol-ene [wt%]
Control TW	–	28 ± 2	0	72 ± 2
TW – Cat 1M	Cationic 1M (24 h)	28 ± 2	4.8 ± 0.3	67 ± 3
TW – Cat 2M	Cationic 2M (24 h)	28 ± 2	4.8 ± 0.4	67 ± 2
TW – An 1M	Anionic 1M (24 h)	28 ± 2	0.56 ± 0.2	71 ± 2
TW – An 2M	Anionic 2M (24 h)	28 ± 2	0.57 ±0.2	71 ± 3

respectively. The low silica content anionic silica 2 M treated balsa TW did not show any observable difference in mechanical properties to the control balsa – TW, but the 2 M cationic silica treated balsa – TW (with 12 ± 1 wt% wood content, 5 ± 1 wt% silica and 83 ± 2 wt. % thiol-ene content) showed increased tensile strength and modulus of 64.3 ± 2 MPa and 4.3 ± 0.3 GPa, respectively. The slight increase in stiffness was observed irrespective of the wood species in the cationic silica sol treated wood samples.

The effective reinforcement modulus (E_{fL}) of cell wall based on rule of mixtures (calculation details under Table S1, Supporting Information) was used to compare the cell wall stiffness in the composites.[65] Increase in E_{fL} was observed in both birch and balsa TW samples containing 2 M cationic silica. Silica has a modulus of 71 GPa, which provides a reinforcement effect although particles are spherical, but a property contribution from ionic bond linking of wood cell wall components can also help.[66]

Freeze fracture cross-sections of the samples showed slightly less fiber pull out in the TW – Cat 2M compared to control TW samples, see Figure S4 (Supporting Information). However, the difference was not significant, so there is no strong effect from silica on polymer-wood interface strength.

2.5. Flame Retardant Properties of Silica – TW Composites

The flame retardant (FR) properties were improved by the addition of silica NPs. The resistance to a burning flame was evaluated in the horizontal configuration shown in **Figure 5**a, where the TW – Cat 2M showed excellent flame retardant properties compared to the control TW. The main result is that the TW becomes self-extinguishing due to the NPs, due to the formation of a surface barrier layer of silica, which protected the layers underneath, as described below. Table S2 (Supporting Information), collects flammability parameters.

The neat reference sample of bleached birch ignites immediately with a burning time of 2.7 ± 0.4 s. The flame is not extinguished until it reaches the clamps, followed by an afterglow effect, arising from nonflaming combustion (i.e., oxidation in the solid state with emission of light). The sample leaves a charred residue of 11 wt%.[67] The addition of 18 ± 5 wt% silica to the bleached wood changes the burning behavior of wood by reducing flame propagation rate and increasing the final residue to 33%. This behavior can be ascribed to a "barrier" effect exerted by the inorganic particles which slows down flame propagation, while favoring the production of charred residue, less prone to afterglow. Flame testing of the control TW leaves a higher residue (Figure S5 and Table S2, Supporting Information), compared to that of control wood or thiolene film of the same volume.

In stark contrast, the TW – Cat 2M modified by silica NPs, showed self-extinguishing characteristics. Regions close to the surfaces exposed to the flame were partly degraded, whereas the inner part of the structure remained completely intact, as evidenced by scanning electron microscopy (SEM) images (Figure 5b,c). On exposure to flame, the volatiles from cellulose and thiol-ene decomposition initially evaporate at the flame-exposed surface to feed the flame. Enrichment of silica NPs then leads to the formation of a protective silica surface layer/coating. Not only is evaporation of volatiles substantially limited, but the barrier may also result in insufficient oxygen availability for the thermo-oxidation of the interior of the composite. This mechanism is supported by EDS mapping data (Figure 5c) showing a dense, neat silica surface. It was observed that the outer wood/thiol-ene layers are degraded by the flame, while the internal portion of the sample is left undamaged.[68,69] The ability of silica to control mass and heat transfer to/from the flame is further corroborated by a previous study where conventional wood was impregnated by silica sols at different

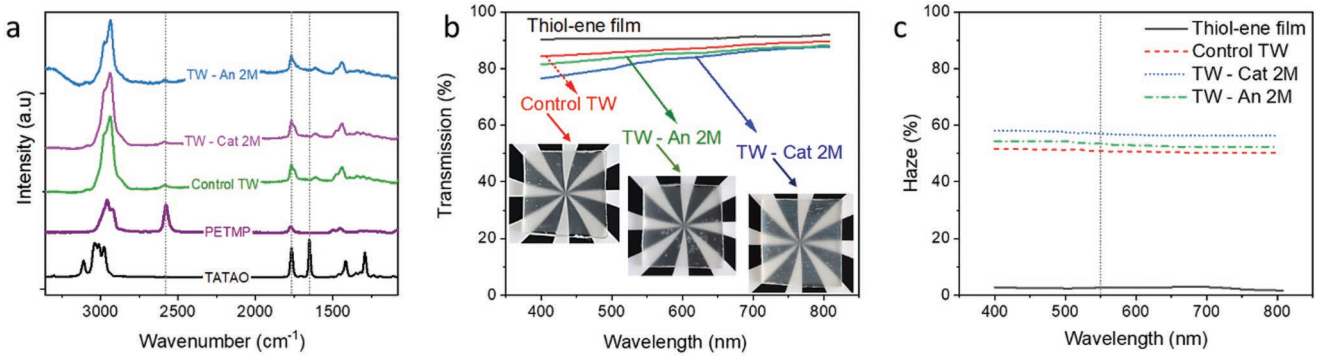

Figure 3. a) Raman spectra of thiol-ene monomers and TW composites. The gray lines correspond to thiol stretching (2572 cm^{-1}), ketone stretching (1765 cm^{-1}), and allyl bending (1650 cm^{-1}) b) and c) represent the transmittance and haze of silica TW composites, respectively. Insets in b) show images of corresponding TW composites. Note compositions in Table 2, where wood content is 28 ± 2 wt% in all composites and silica content 4.8 ± 0.4 wt% for silica NPs in TW – Cat 2M.

Table 2. Quantification of degree of cure for neat polymer (neat thiol-ene) and TW composites.

	Neat thiol-ene	Thiol-ene TW		TW – Cat 2M		TW – An 2M	
		Lumen	Cell wall	Lumen	Cell wall	Lumen	Cell wall
Thiol [%]	92.0 ± 0.2	96.4 ± 0.3	92.0 ± 0.1	96.2 ± 0.2	92.2 ± 0.3	96.1 ± 0.1	92.1 ± 0.2
ene [%]	93.1 ± 0.1	99.0 ± 0.2	100	99.1 ± 0.1	100	99.0 ± 0.2	100

concentrations showing strong effects on burning rates of the prepared samples.[70] In addition it is worth mentioning that the thiolene used in this system showed slower burning rate compared to a poly(methyl methacrylate) (PMMA) film, depicting a better choice of polymer compared to PMMA, often used for TW composites, Table S2 (Supporting Information).

In order to investigate further on the FR properties of the prepared TW, cone calorimetry tests have been performed. The main plots from cone calorimetry tests are reported in Figure S6 (Supporting Information), while the measured parameters are collected in Table S3 (Supporting Information). Bleached birch and TW are employed as control samples for their cationic silica containing counterparts. Overall, the presence of the thiol-ene polymer is responsible for increased heat release rate HRR and smoke parameters. This is expected and related to the substantial differences in composition and density between bleached samples and TW. Interestingly, the presence of silica is found to influence smoke production. Indeed, total smoke release TSR values of both bleached birch Cat 2M and TW – Cat 2M are reduced with respect to their control samples (–78% and –23%, respectively). In addition, for TW samples, time to ignition TTI values are also increased (+15 s). On the other hand, pkHRR values appear to be slightly increased while remaining within the accepted experimental error for cone calorimetry tests. The presence of small cracks in the protective silica rich layer could act as preferential channels through which the combustible volatiles concentrate and leak. This can result in the increase in HRR values.[71] The presence of silica also helped in partially preserving dimensional stability of the charred residue after combustion as shown in Figure S6b (Supporting Information). It seems that the inclusion of silica has little effect in reducing HRR parameters, while helping performance by contributing to increased TTI and reduced TSR.

It is concluded that inclusion of cationic silica resulted in improved FR performance. The approach is unique in that it exploits the nanostructuration of the wood template cell walls so that a small amount of silica can have a strong effect. The reason is its tailored distribution only in the closed cell wood "skeleton" penetrating the whole material. Other FR approaches recently proposed involve strategies based on either the inclusion of conventional FR chemicals such as ammonium polyphosphate in the impregnating monomer or the use of an intrinsic FR polymer, such as a polyimide. [72,73] Although forced combustion tests by cone calorimetry were not performed, the referenced approaches produced TW with self-extinguishing behavior during flammability tests as also demonstrated by the present paper. One of the advantages of the proposed approach is the versatility of the process that opens for implementation of a plethora of water-born and sustainable FR chemicals without the need to modify the impregnating polymer.

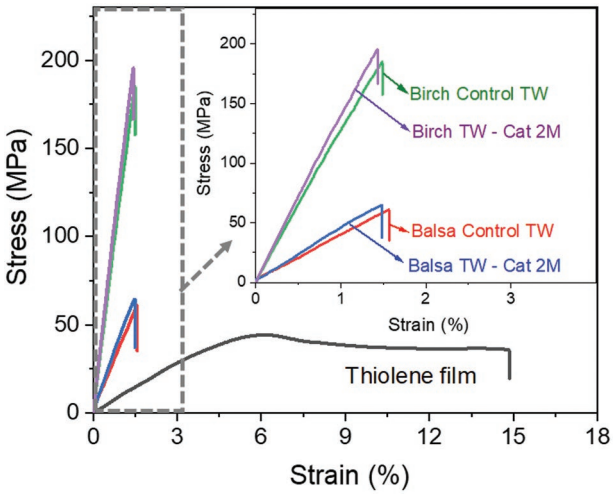

Figure 4. Stress–strain curves of TW composites and neat thiol-ene films tested in the grain (fiber) direction.

3. Conclusions

The diffusion and migration of NPs to the wood substrate was correlated with the charge densities of the wood and silica particles, in support of the hypothesis of uniform distribution of silica achieved by efficient electrostatic interactions. At an aqueous pH of 8.5, the wood cell wall is swollen and the electrostatic wood-NP charge differences influence the infiltration of silica NPs into wood. This opens the possibility to expand this nanotechnology to a wide range of NPs for wood functionalization in a scalable process without the need of any chemical wood modification. Also, a high NP content (≈20 wt% of wood) is achieved with uniform diffusion and NP distribution. SEM and EDS analysis confirmed details of the uniform distribution of silica across the cross-sections. The transmission and haze of the formed TW are not strongly influenced, which suggests that scattering takes place at wood-polymer interfaces rather than inside the wood cell wall. The addition of 4.8 wt% of silica (in the TW composite) increased the modulus by ≈ 11% in TW – Cat 2M. This low addition of silica resulted in dramatically improved flame retardant properties in the TW – Cat 2M composites. A dense, silica-rich surface layer is formed so that the inner material is protected by oxygen depletion and slow release of volatile degradation products. Wood biocomposite functionality can certainly be enhanced by facile impregnation of NPs into wood and wood cell walls by the use of charge interaction mechanisms.

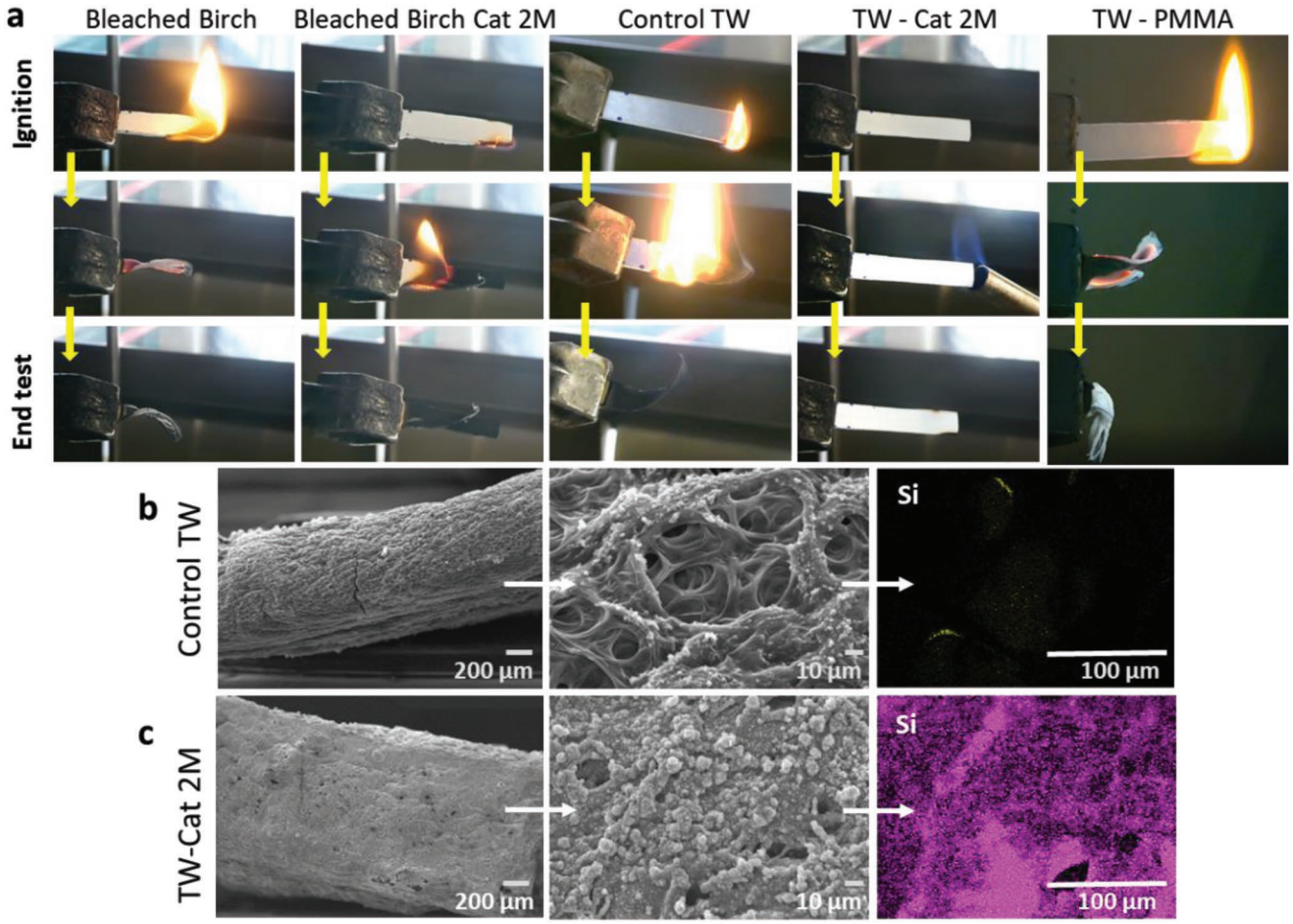

Figure 5. Flame retardant characterization: a) snapshots from flammability test, SEM cross sectional micrographs of b) control TW and c) TW – Cat 2M silica residues along with the Si EDS mapping. EDS mapping of the TW – Cat 2M residue show the protective layer of silica.

4. Experimental Section

Materials: Balsa wood with density of 170–200 kg m^{-3} was procured from Material AB (Sweden). Birch wood (Betula Pendula) with density 530 kg m^{-3} was purchased from Sydfanér AB (Sweden). Acetone, ethanol absolute (99%) and sodium hydroxide were supplied from VWR. Hydrogen peroxide (30%), UV initiator 1-hydroxycyclohexyl phenyl ketone, pentaerythritoltetrakis (3-mercaptopropionate) (PETMP, tetra functional thiol monomer), sodium acetate, sodium silicate and 1,3,5-trially-1,3,5-trione-2,4,6(1H,3H,5H)-triazine (TATATO) were supplied from Sigma-Aldrich, Sweden. Acetic acid (Honeywell), diethylallyltriaminepenta acetic acid (DTPA, Acros Organics), magnesium sulfate (Scharlau), and sodium chlorite (40%, Alfa Aesar) were procured and used as received. Silica NPs with size of 30 ± 5 nm (measured from DLS) had a specific surface of 85 m^2 g^{-1}, as reported by the supplier were received from Nouryon, Bohus, Sweden under the tradename of Levasil CS45-58P and CS45-38P. Levasil CS45-58P is modified with aluminum chlorohydrate. The presence of positive aluminum units are considered to generate the cationic charges. CS45-38P is the anionic version where the dissociation of the silanol groups create the anionic charges. The refractive index value of silica was reported to be 1.45, as notified by the supplier. Milli-Q water was used for preparation of the formulations. The zeta potential values of cationic silica sol at concentrations of 0.17, 1, and 2 M are 50.1 ± 1 mV, measured at pH 8.5 using Nano ZS Malvern Dynamic Light Scattering meter (Zetasizer) Instrument.

Lignin Modification of Wood (Bleaching): Native wood in dimensions of 15×15×1.1 or 100×100×1.1 mm^3 (for silica retainment studies) were weighed and treated with an aqueous hydrogen peroxide based bleaching solution at 70 °C. The bleaching solution consisted of sodium silicate 3.0 weight (wt%), sodium hydroxide (3.0 wt%), magnesium sulfate (0.1 wt%), DTPA (0.1 wt%), and hydrogen peroxide (4.0 wt%) in de-ionized (DI) water as per the process reported elsewhere.[19] Samples were treated until they turned visibly white.

Infiltration of Silica NPs into Wood: Measured volume of bleached birch was immersed inside 0.17, 1, and 2 M of cationic or anionic silica sols for 48 h or otherwise stated while maintaining a wood to silica sol weight ratio of 1:5. Samples were washed thoroughly with deionized water and rinsed for 5 times to remove surface deposited silica.

Fabrication of Transparent Wood: Bleached wood samples were washed with deionized water and were solvent exchanged with ethanol and acetone. These wood templates were then infiltrated with stoichiometric mixtures of thiol and allyl functionalized monomers of PETMP and TATATO, respectively, containing UV-initiator 1-hydroxycyclohexyl phenyl ketone (0.5 wt%) under vacuum for 24 h. Acetone present in the samples evaporated during the vacuum infiltration process. Samples were additionally kept at 50 °C for 30 min to remove residual acetone, monitored by weight loss assessment. Monomer infiltrated samples were then sandwiched between two glass slides and cured for 4 min by illumination from four 9 W 365 nm UV-lamps: two on opposite sides of and two above the sample to ensure uniform curing. Mass fraction of

wood and polymer in the resultant composites were determined from the density difference between bleached and the cured TW samples after drying the bleached samples at 105 ± 3 °C for 24 h. Scheme 1 represents the fabrication process for TW composites. Samples treated with silica sol were treated in the similar process to generate silica loaded TW.

Characterization: Silica sol treated wood samples were washed thoroughly with DI water to get rid of surface adhered loose NPs, before analyzing their properties.

The infiltration of silica inside the wood was determined from the oven dried weight difference between bleached and silica impregnated bleached samples after thorough DI washing for sample dimensions of 100×100×1.1 mm^3 (5 replicas of each sample).

Morphology of the TW composites and the interfacial polymer-wood bonding was analyzed using field-emission scanning electron microscopy (FE-SEM, Hitachi S-4800) operating at accelerating voltage of 1.0 kV and a working distance of 9.8 mm. Samples were cryo-fractured in liquid nitrogen before analyzing their cross-sections. Elemental analyses of the cryo fractured cross-sections of samples were carried out using EDX spectroscopy (Oxford Instruments, X-MAX N 80, UK) operating at an accelerating voltage of 10 kV with working distance of 15 mm.

The particle size (presented as diameter) and zeta potential measurements were performed using dynamic light scattering (DLS) (Zetasizer ZEN3600, Malvern Instruments Ltd. UK). Disposable folded capillary cells were used for size as well as zeta potential analysis. The measurements were repeated three times with 50 runs per measurement.

Raman spectra were measured for the freeze fractured cross-sections from TW samples, using confocal Raman microscopy (Jobin Yvon HR800 UV, Horiba) together with a light source from a 514 nm laser (Stellar-Pro, Modu-laser) and a mechanized stage. Spectra were averaged from 10 scans and analyzed for comparison. The degree of cure of the monomers in the TW composites were analyzed as per procedure detailed elsewhere.[20,63]

Tensile tests were performed using an Instron 5944 (USA) instrument equipped with a 2 kN load cell, with sample dimensions of 50×5×1 mm^3. The tests were carried out in the longitudinal axis along the fiber direction with a strain rate of 10% min^{-1} and gauge length of 25 mm. Samples were preconditioned for 24 h and tested in a room at a temperature of 22 ± 1 °C with 50 ± 2% relative humidity. 10 replicas of each sample were measured and the average values are reported.

Optical measurements were performed using an integrating sphere in the visible and NIR wavelength region (400–1000 nm) according to ASTM D1003, Standard Method for Haze and Luminous Transmittance of Transparent Plastics.[74] A laser-driven xenon plasma white-light source (Energetiq EQ-99) coupled with a tunable monochromator (SP2150i, Princeton Instruments) was used as excitation source, a 6 in. diameter integrating sphere (Labsphere) provides light collection, and the Peltier element cooled CCD camera (–75 °C) is connected to a spectrometer for the signal acquisition. The setup components were connected to the integrating sphere with multimode optical fibers. The system response curve was obtained by using excitation source with a monochromator, where a calibration was performed with an optical power meter (Newport). The sample was placed in front of an input port of the integrating sphere. 3 replicas of each sample were measured, and the results were statistically averaged. Briefly, four measurements were performed for calculating the transmittance and haze, as represented in **Table 3**. The background noise was subtracted before calculating the transmittance and haze values.

Then transmittance and haze of the TWC samples were calculated as

$$\text{Transmittance}(\lambda) = \frac{S_2(\lambda)}{S_1(\lambda)} \tag{1}$$

$$\text{Haze}(\lambda) = \frac{S_3(\lambda)}{S_2(\lambda)} - \frac{S_4(\lambda)}{S_1(\lambda)} \tag{2}$$

The charge of anionic samples was determined by polyelectrolyte titration with the help of a Stabino particle charge titrator (Particle Metrix Gmbh, Meerbusch, Germany), using 400–500 kDa poly (diallyldimethylammonium chloride) (PDADMAC) (Ciba, Yorkshire, UK) as a titrant, at concentrations of 0.347 µmol mL^{-1}. Potassium polyvinyl sulfate (KPVS) (Wako, Japan) at concentration of 0.3635 µmol mL^{-1} was used as a titrant for determining the charge of cationic samples. Measured volume of silica sol either cationic or anionic of known concentrations were diluted with 10 mL of Milli-Q water. This solution was then titrated with oppositely charged titrant and the equivalent volume of titrant consumed to neutralize the charge was measured. Charge of the sample in micro equivalent (micro eq.) was obtained from the product of charge of the titrant solution (micro eq. mL^{-1}) and equivalent volume of the consumed titrant to neutralize the charge (mL). Charge density of the sample (micro eq. g^{-1}) was determined by dividing the charge of sample (micro eq.) by the product of volume of sample used for titration (mL) and concentration of the sample (g mL^{-1}). 15×15×1.1 mm^3 of wet bleached wood was immersed in a 10 mL of silica sol with predetermined concentration and charge density at pH 8.5. The charge of the sol was monitored after regular time intervals. An average of 4 measurements for each experiment was reported.

For flammability assessment, the resistance against application of flame and the subsequent combustion behavior was evaluated by flammability test in horizontal configuration. Each sample (50×10×1 mm^3) was mounted in horizontal configuration and ignited from its short side by a 20 mm blue methane flame with a flame application time of 3 s. The test was repeated 3 times for each formulation to ensure reproducibility. During the test, burning time, time to end test, and final residue, were registered. The combustion behavior of square samples (50×50×2 mm^3) was investigated by means of cone calorimetry tests (Noselab, ats-fire testing) under 35 kW m^{-2} heat flux. Three samples per formulation were tested evaluating: Time to Ignition (TTI, s), average and peak and time to peak of Heat Release Rate (avHRR, pkHRR, kW m^{-2}, TpkHRR, s), Total Heat Release (THR, MJ m^{-2}), Total smoke release (TSR, m^2 m^{-2}), and final residue. Average values and plots are reported. Prior flammability cone calorimetry tests, samples were conditioned in climatic chamber at 23 °C and 50% relative humidity for 24 h. The morphology of postcombustion residues from flammability tests was investigated using EVO15 (Zeiss, Germany) scanning electron microscope (beam voltage 20 kV), equipped with probe (Oxford Ultimax 40) for elemental analysis. The cross-section of the samples was positioned on conductive tape and gold sputtered before the measurements.

The wood silica interactions were analyzed using FTIR instrument spectrum 100 from Perkin Elmer with an attachment of MKII Golden

Table 3. Transmittance and haze reading correspondences.

Reading designation	Specimen in position	Light trap in position	Reflectance standard in position	Quantity represented
S1	No	No	Yes	Incident light
S2	Yes	No	Yes	Total light transmitted by specimen
S3	Yes	Yes	No	Light scattered by specimen and instrument
S4	No	Yes	No	Light scattered by instrument

Gate and an ATR diamond crystal (Graseby Specac Ltd. UK). The FTIR spectra were recorded at room temperature from 600 to 4000 cm^{-1}.

Supporting Information

Supporting Information is available from the Wiley Online Library or from the author.

Acknowledgements

Erik Jungstedt is acknowledged for assistance in mechanical property analysis. Peter Olsén is acknowledged for constructive discussions for FTIR analysis. This project has received funding from the European Research Council (ERC) under the European Union's Horizon 2020 research and innovation programme (Grant Agreement No. 742733, Wood NanoTech) and from Knut and Alice Wallenberg foundation through the Wallenberg Wood Science Center.

Conflict of Interest

The authors declare no conflict of interest.

Data Availability Statement

The data that support the findings of this study are available in the supplementary material of this article.

Keywords

biocomposites, charge density, flame retardant, silica, transparent wood

Received: September 24, 2021
Revised: January 7, 2022
Published online: January 27, 2022

[1] D. Trache, A. F. Tarchoun, M. Derradji, T. S. Hamidon, N. Masruchin, N. Brosse, M. H. Hussin, *Front. Chem.* **2020**, *8*, 392.
[2] T. C. Mokhena, E. R. Sadiku, M. J. Mochane, S. S. Ray, M. J. John, A. Mtibe, *Carbohydr. Polym.* **2021**, *273*, 118507.
[3] C. Goldhahn, E. Cabane, M. Chanana, *Philos. Trans. R. Soc. A* **2021**, *379*, 20200339.
[4] Z. Zhu, G. Xiao, J. Chen, S. Fu, *Cellulose* **2020**, *27*, 8513.
[5] N. Ijaz, F. Dai, Z. Rehman, *J. Environ. Manage.* **2020**, *262*, 110285.
[6] Z. Cheng, H. Guan, J. Meng, X. Wang, *ACS Omega* **2020**, *5*, 14096.
[7] C. Gusenbauer, E. Cabane, N. Gierlinger, J. Colson, J. Konnerth, *Sci. Rep.* **2019**, *9*, 18569.
[8] C. Montanari, P. Olsén, L. A. Berglund, *Green Chem.* **2020**, *22*, 8012.
[9] C. Kaldun, S. Dahle, W. Maus-Friedrichs, J. C. Namyslo, D. E. Kaufmann, *Holzforschung* **2016**, *70*, 411.
[10] R. Mi, T. Li, D. Dalgo, C. Chen, Y. Kuang, S. He, X. Zhao, W. Xie, W. Gan, J. Zhu, J. Srebric, R. Yang, L. Hu, *Adv. Funct. Mater.* **2020**, *30*, 1907511.
[11] H. S. Yaddanapudi, N. Hickerson, S. Saini, A. Tiwari, *Vacuum* **2017**, *146*, 649.
[12] X. Wang, T. Zhan, Y. Liu, J. Shi, B. Pan, Y. Zhang, L. Cai, S. Q. Shi, *ChemSusChem* **2018**, *11*, 4086.
[13] C. J. Brett, W. Ohm, B. Fricke, A. E. Alexakis, T. Laarmann, V. Körstgens, P. Müller-Buschbaum, L. D. Söderberg, S. V. Roth, *ACS Appl. Mater. Interfaces* **2021**, *13*, 27696.
[14] H. Zhu, W. Luo, P. N. Ciesielski, Z. Fang, J. Y. Zhu, G. Henriksson, M. E. Himmel, L. Hu, *Chem. Rev.* **2016**, *116*, 9305.
[15] Y. Yang, L. Shan, H. Shen, J. Qiu, *Prog. Org. Coat.* **2021**, *154*, 106186.
[16] R. Mi, C. Chen, T. Keplinger, Y. Pei, S. He, D. Liu, J. Li, J. Dai, E. Hitz, B. Yang, I. Burgert, L. Hu, *Nat. Commun.* **2020**, *11*, 3836.
[17] U. Müller, M. Rätzsch, M. Schwanninger, M. Steiner, H. Zöbl, *J. Photochem. Photobiol., B* **2003**, *69*, 97.
[18] T. K. Das, A. K. Jain, *Environ. Prog.* **2001**, *20*, 87.
[19] Y. Li, Q. Fu, R. Rojas, M. Yan, M. Lawoko, L. Berglund, *ChemSusChem* **2017**, *10*, 3445.
[20] A. Samanta, H. Chen, P. Samanta, S. Popov, I. Sychugov, L. A. Berglund, *ACS Appl. Mater. Interfaces* **2021**, *13*, 3270.
[21] V. Merk, M. Chanana, S. Gaan, I. Burgert, *Holzforschung* **2016**, *70*, 867.
[22] M. Höglund, J. Garemark, M. Nero, T. Willhammar, S. Popov, L. A. Berglund, *Chem. Mater.* **2021**, *33*, 3736.
[23] C. A. Clausen, F. Green, S. N. Kartal, *Nanoscale Res. Lett.* **2010**, *5*, 1464.
[24] P. Olsén, N. Herrera, L. A. Berglund, *Biomacromolecules* **2020**, *21*, 597.
[25] B. M. Weight, A. R. Denton, *J. Chem. Phys.* **2018**, *148*, 114904.
[26] K. van Gruijthuijsen, M. Obiols-Rabasa, M. Heinen, G. Nägele, A. Stradner, *Langmuir* **2013**, *29*, 11199.
[27] C. Schneider, M. Hanisch, B. Wedel, A. Jusufi, M. Ballauff, *J. Colloid Interface Sci.* **2011**, *358*, 62.
[28] J. S. Segmehl, A. Lauria, T. Keplinger, J. K. Berg, I. Burgert, *Front. Chem.* **2018**, *6*, 28.
[29] J. Jiang, J. Cao, W. Wang, *De Gruyter Holzforsch.* **2018**, *72*, 311.
[30] O. Nechyporchuk, H. Ulmefors, A. Teleman, *Carbohydr. Polym.* **2021**, *264*, 118032.
[31] S. Hasebe, S. Aoyama, M. Tanaka, H. Kawakami, *J. Membr. Sci.* **2017**, *536*, 148.
[32] M. Najafi, M. Sadeghi, A. Bolverdi, M. Pourafshari Chenar, M. Pakizeh, *Adv. Polym. Technol.* **2018**, *37*, 2043.
[33] M. Rodríguez-Robledo, M. González-Lozano, P. Ponce-Peña, P. Q. Owen, M. Aguilar-González, G. Nieto-Castañeda, E. Bazán-Mora, R. López-Martínez, G. Ramírez-Galicia, M. Poisot, *Materials* **2018**, *11*, 575.
[34] M. P. Gashti, F. Alimohammadi, A. Shamei, *Surf. Coat. Technol.* **2012**, *206*, 3208.
[35] X. Mu, Y. Xiao, W. Cai, Z. Yulu, W. Wang, X. Li, X. Wang, L. Song, *J. Colloid Interface Sci.* **2022**, *605*, 241.
[36] E. Gibertini, F. Carosio, K. Aykanat, A. Accogli, G. Panzeri, L. Magagnin, *Surf. Interfaces* **2021**, *25*, 101252.
[37] J. Cao, M. Xiaolong, A. Yang, W. Xu, *Polym. Polym. Compos.* **2006**, *14*, 65.
[38] B. Xiang, R. Zhang, Y. Luo, S. Zhang, L. Xu, H. Min, S. Tang, X. Meng, *Nano Energy* **2021**, *81*, 105600.
[39] F. Wahid, X.-J. Zhao, Y.-X. Duan, X.-Q. Zhao, S.-R. Jia, C. Zhong, *Carbohydr. Polym.* **2021**, *257*, 117611.
[40] I. Prihatiningtyas, Y. Hartanto, M. S. R. Ballesteros, B. Van der Bruggen, *J. Appl. Polym. Sci.* **2021**, *138*, 50000.
[41] T. Peng, J. Zhu, T. Huang, C. Jiang, F. Zhao, S. Ge, L. Xie, *J. Appl. Polym. Sci.* **2021**, *138*, 50539.
[42] S. Kunjalukkal Padmanabhan, C. Protopapa, A. Licciulli, *Process Biochem.* **2021**, *103*, 31.
[43] D. Wang, X. Feng, L. Zhang, M. Li, M. Liu, A. Tian, S. Fu, *Chem. Eng. J.* **2019**, *375*, 121933.
[44] J. Wiegmann, *Acta Polym.* **1980**, *31*, 406.
[45] X. Hu, Z. Sun, *J. Build. Eng.* **2021**, *44*, 102987.
[46] L. Zhang, Y. Huang, P. Sun, Y. Hai, S. Jiang, *Soft Matter* **2021**, *17*, 5231.

[47] F. Solis-Pomar, A. Díaz-Gómez, M. E. Berrío, J. Ramírez, A. F. Jaramillo, K. Fernández, D. Rojas, M. F. Melendrez, E. Pérez-Tijerina, *Coatings* **2021**, *11*, 460.
[48] F. Sohbatzadeh, A. Shabannejad, M. Ghasemi, Z. Mahmoudsani, *Prog. Org. Coat.* **2021**, *151*, 106070.
[49] C. Liang, Y. Du, Y. Wang, A. Ma, S. Huang, Z. Ma, *Adv. Compos. Hybrid Mater.* **2021**, *4*, 979.
[50] L. Yan, Z. Xu, X. Wang, *J. Therm. Anal. Calorim.* **2019**, *136*, 1563.
[51] S. Gebke, K. Thümmler, R. Sonnier, S. Tech, A. Wagenführ, S. Fischer, *Molecules* **2020**, *25*, 335.
[52] L. Lowden, T. Hull, *Fire Sci. Rev.* **2013**, *2*, 4.
[53] A. Salamova, R. A. Hites, *Environ. Sci. Technol.* **2013**, *47*, 349.
[54] B. Mahltig, C. Swaboda, A. Roessler, H. Böttcher, *J. Mater. Chem.* **2008**, *18*, 3180.
[55] Y.-J. Kim, M. Osako, S. Sakai, *Chemosphere* **2006**, *65*, 506.
[56] M. M. Lounasvuori, K. B. Holt, *Chem. Commun.* **2017**, *53*, 2351.
[57] M. Namazian, S. Halvani, *J. Chem. Thermodyn.* **2006**, *38*, 1495.
[58] L. Hu, M. Du, J. Zhang, *Open J. For.* **2018**, *08*, 15.
[59] J. J. Howard, J. S. Perkyns, B. M. Pettitt, *J. Phys. Chem. B* **2010**, *114*, 6074.
[60] V. Pushpamalar, S. J. Langford, M. Ahmad, Y. Y. Lim, *Carbohydr. Polym.* **2006**, *64*, 312.
[61] S. Iqbal, J.-I. Yun, *Microporous Mesoporous Mater.* **2017**, *248*, 149.
[62] A. Daochalermwong, N. Chanka, K. Songsrirote, P. Dittanet, C. Niamnuy, A. Seubsai, *ACS Omega* **2020**, *5*, 5285.
[63] M. Höglund, M. Johansson, I. Sychugov, L. A. Berglund, *ACS Appl. Mater. Interfaces* **2020**, *12*, 46914.
[64] Y. Li, E. Vasileva, I. Sychugov, S. Popov, L. Berglund, *Adv. Opt. Mater.* **2018**, *6*, 1800059.
[65] E. Jungstedt, C. Montanari, S. Östlund, L. Berglund, *Composites, Part A* **2020**, *133*, 105853.
[66] L. B. Freund, S. Suresh, *Thin Film Materials: Stress, Defect Formation and Surface Evolution*, 1st ed., Cambridge University Press, Cambridge **2004**.
[67] A. Anca-Couce, N. Zobel, A. Berger, F. Behrendt, *Combust. Flame* **2012**, *159*, 1708.
[68] F. Carosio, L. Maddalena, J. Gomez, G. Saracco, A. Fina, *Adv. Mater. Interfaces* **2018**, *5*, 1801288.
[69] F. Carosio, A. Di Blasio, F. Cuttica, J. Alongi, A. Frache, G. Malucelli, *Ind. Eng. Chem. Res.* **2013**, *52*, 9544.
[70] M. Pries, C. Mai, *Eur. J. Wood Prod.* **2013**, *71*, 237.
[71] J. Alongi, F. Carosio, G. Malucelli, *Cellulose* **2012**, *19*, 1041.
[72] A. Aldalbahi, M. E. El-Naggar, T. A. Khattab, M. Hossain, *Luminescence* **2021**, *36*, 1922.
[73] L. Chen, Z. Xu, F. Wang, G. Duan, W. Xu, G. Zhang, H. Yang, J. Liu, S. Jiang, *Compos. Commun.* **2020**, *20*, 100355.
[74] L. Pike, *J. Plast. Film Sheeting* **1993**, *9*, 173.